Causal and Structural Connectivity of Pulse-Coupled Nonlinear Networks

Article *in* Physical Review Letters · August 2013

DOI: 10.1103/PhysRevLett.111.054102 · Source: PubMed

5 authors, including:

Douglas Zhou
Shanghai Jiao Tong University
99 PUBLICATIONS **830** CITATIONS
SEE PROFILE

Yanyang Xiao
Shanghai Jiao Tong University
15 PUBLICATIONS **370** CITATIONS
SEE PROFILE

Yaoyu Zhang
New York University Abu Dhabi
56 PUBLICATIONS **522** CITATIONS
SEE PROFILE

Zhiqin John Xu
Shanghai Jiao Tong University
81 PUBLICATIONS **879** CITATIONS
SEE PROFILE

Causal and Structural Connectivity of Pulse-Coupled Nonlinear Networks

Douglas Zhou,[1] Yanyang Xiao,[1] Yaoyu Zhang,[1] Zhiqin Xu,[1] and David Cai[1,2,3,*]

[1]*Department of Mathematics, MOE-LSC, and Institute of Natural Sciences, Shanghai Jiao Tong University, Shanghai 200240, China*
[2]*Courant Institute of Mathematical Sciences and Center for Neural Science, New York University, New York, New York 10012, USA*
[3]*NYUAD Institute, New York University Abu Dhabi, P.O. Box 129188, Abu Dhabi, United Arab Emirates*

(Received 5 February 2013; revised manuscript received 13 May 2013; published 29 July 2013)

We study the reconstruction of structural connectivity for a general class of pulse-coupled nonlinear networks and show that the reconstruction can be successfully achieved through *linear* Granger causality (GC) analysis. Using spike-triggered correlation of whitened signals, we obtain a quadratic relationship between GC and the network couplings, thus establishing a direct link between the causal connectivity and the structural connectivity within these networks. Our work may provide insight into the applicability of GC in the study of the function of general nonlinear networks.

DOI: 10.1103/PhysRevLett.111.054102 PACS numbers: 05.45.Tp, 02.50.Tt, 05.10.−a, 84.35.+i

For networks in scientific and engineering fields, e.g., genetic regulatory systems, the circuitry in the brain, and social communications, signals are often collected in the form of a time series of dynamical activity at individual nodes. In order to understand how these nodes cooperate to generate specific network functions, a fundamental issue is to identify causal interactions among the nodes [1]. The Granger causality (GC), based on linear predictions, has proven to be an effective method for the analysis of causal interactions among nodes by distinguishing the driver from the recipient [2]. The idea of GC is that the driver, being earlier than the recipient, contains information about the future of the recipient; thus, the prediction error for the recipient is reduced when the information of the driver is incorporated. Because of its simplicity and easy implementation, the GC theory has been widely applied to many scientific problems in, e.g., neuroscience, systems biology, medical engineering, geophysics, economics, and the social sciences [3].

Despite widespread applications of GC theory, there are several important issues that remain to be clarified. First, GC theory is based on linear models and assumes that the causal information can be well captured by the low order statistics (up to the variance) of signals. For Gaussian time series, GC is equivalent to the transfer entropy [4]. However, many experimental time series are nonlinear and non-Gaussian. For example, there is an extensive application of GC analysis to functional magnetic resonance imaging data, which, however, are known to be nonlinear functions of physiological processes [5]. The GC analysis can yield highly significant false detections for data with a mixed source, e.g., electroencephalogram data [6]. Second, the causal connectivity revealed in GC is statistical rather than structural. Strong GC connections may exist between brain regions with no direct structural connections [7], or a network may possess different GC connectivity in different dynamical states [8]. To understand how the causal connectivity is mapped onto the anatomical, i.e., structural, connectivity in the brain remains one of the major challenges in neuroscience [9]. In addition, it has been shown that the GC analysis for some nonlinear systems may lead to an incorrect inference of the structural connectivity [10]. Therefore, it is important to study the applicability of GC theory for nonlinear network systems [11] and to investigate the relationship between the structural connectivity and the GC connectivity.

In this Letter, we consider a general class of pulse-coupled nonlinear networks. These systems arise from many research fields, e.g., image processing, path optimization, speech recognition, gene regulatory modeling, and neuronal dynamics [12]. Using nonlinear and non-Gaussian time series generated by such networks, we show that the GC connectivity is highly coincident with the structural connectivity over a wide range of dynamical regimes. Namely, the network topology, which is usually not easy to assess in experiment, can be accurately reconstructed from time series recorded at individual nodes. Our theoretical analysis reveals why the linear GC framework is applicable to such a nonlinear network and how the causal interaction is quantitatively related to the coupling strength of the network. We also point out that the spike-triggered correlation (STC), a classical technique to detect dynamical interactions between nodes, may incorrectly infer connections if the signals are not white. Our work provides a theoretical framework for understanding the validity of GC theory in nonlinear networks and may provide insight into how information is propagated over a network and how the structural and functional properties are related.

The system we consider is an integrate-and-fire (I&F) network with both excitatory and inhibitory nodes. The dynamics of the ith node is governed by

$$\dot{x}_i = -\frac{x_i}{\tau} - (g_i^{\mathrm{bg}} + g_i^{\mathrm{ex}})(x_i - x_{\mathrm{ex}}) - g_i^{\mathrm{in}}(x_i - x_{\mathrm{in}}), \quad (1)$$

where x_i is a state variable with time scale τ, and x_{ex} and x_{in} are the reversal values of excitation (ex) and inhibition (in),

respectively. $g_i^{\rm bg} = f\sum_k H(t - T_{i,k}^F)\exp[-(t - T_{i,k}^F)/\sigma^{\rm ex}]$ is the background input with magnitude f and time scale $\sigma^{\rm ex}$, $T_{i,k}^F$ is a Poisson process with rate μ, $H(\cdot)$ is the Heaviside function, $g_i^{\rm ex} = \sum_j \sum_k S_{ij}^{\rm ex} H(t - T_{j,k}^{\rm ex})\exp[-(t - T_{j,k}^{\rm ex})/\sigma^{\rm ex}]$ is the excitatory pulse interaction from other jth excitatory nodes, and $g_i^{\rm in} = \sum_j \sum_k S_{ij}^{\rm in} H(t - T_{j,k}^{\rm in})\exp[-(t - T_{j,k}^{\rm in})/\sigma^{\rm in}]$ is the inhibitory pulse interaction from other jth inhibitory nodes. The jth excitatory (inhibitory) node x_j evolves continuously according to Eq. (1) until it reaches a firing threshold $x_{\rm th}$. That moment in time is referred to as a firing event (say, the kth spike) and denoted by $T_{j,k}^{\rm ex}$ ($T_{j,k}^{\rm in}$). Then, x_j is reset to the reset value x_r ($x_{\rm in} < x_r < x_{\rm th} < x_{\rm ex}$) and held at x_r for an absolute refractory period of $\tau_{\rm ref}$. Each spike emerging from the jth excitatory (inhibitory) node gives rise to an instantaneous increase $S_{ij}^{\rm ex}$ ($S_{ij}^{\rm in}$) in $g_i^{\rm ex}$ ($g_i^{\rm in}$), where $S_{ij}^{\rm ex}$ and $S_{ij}^{\rm in}$ are the excitatory and inhibitory coupling strengths, respectively. The model (1) describes a general class of physical networks [12,13]. In the limit $\sigma^{\rm ex} \to 0$, $\mu \to \infty$ and $g_i^{\rm in} \equiv 0$, $\mu f = {\rm const}$, it reduces to Mirollo-Strogatz oscillators which are widely used in the study of synchronization phenomena [12]. The model is also commonly used as a conductance-based neuronal unit [13]. [For ease of discussion, we will call a node here a neuron, x_i the voltage, and $g_i^{\rm ex}$ ($g_i^{\rm in}$) the excitatory (inhibitory) conductance.]

We address the issue of whether the linear GC framework can be used to reconstruct the connectivity matrices $S_{ij}^{\rm ex}$ and $S_{ij}^{\rm in}$ of the I&F network (1). For simplicity, we first consider a homogeneously coupled network with only excitatory nodes, i.e., $g_i^{\rm in} \equiv 0$ and $S_{ij}^{\rm ex} = S^{\rm ex} A_{ij}$, where $S^{\rm ex}$ is the coupling strength and $\mathbf{A} = (A_{ij})$ is the adjacency matrix characterizing the directed graph among the nodes. For the system of two neurons (x_1 and x_2), we record the time series $\{x_i(n)\}_{n=1}^{\infty}$ ($i = 1, 2$) from their trajectories obtained by evolving system (1) numerically. The autoregressions (AR) for $x_i(n)$ are represented by $x_1(n) = \sum_k a_k^A x_1(n - k) + \epsilon_n^A$ and $x_2(n) = \sum_k d_k^A x_2(n - k) + \eta_n^A$, whereas the joint regressions (JR) can be expressed as $x_1(n) = \sum_k a_k^J x_1(n - k) + \sum_k b_k^J x_2(n - k) + \epsilon_n^J$ and $x_2(n) = \sum_k c_k^J x_1(n - k) + \sum_k d_k^J x_2(n - k) + \eta_n^J$. Here, (ϵ_n^A, η_n^A) and (ϵ_n^J, η_n^J) are residuals in the AR and JR models, respectively [14]. The GC from $\mathbf{x}_1$ to $\mathbf{x}_2$ is defined as $F_{\mathbf{x}_1 \to \mathbf{x}_2} = \ln({\rm Var}(\eta^A)/{\rm Var}(\eta^J))$ and the GC from $\mathbf{x}_2$ to $\mathbf{x}_1$ as $F_{\mathbf{x}_2 \to \mathbf{x}_1} = \ln({\rm Var}(\epsilon^A)/{\rm Var}(\epsilon^J))$ [2]. For the directed network shown in Fig. 1(a), we obtain that $F_{\mathbf{x}_1 \to \mathbf{x}_2} \gg F_{\mathbf{x}_2 \to \mathbf{x}_1}$ ($F_{\mathbf{x}_1 \to \mathbf{x}_2} = 2.0 \times 10^{-4}$ and $F_{\mathbf{x}_2 \to \mathbf{x}_1} = 2.0 \times 10^{-6}$ within statistical error). According to the large-sample distribution theory, the sample statistic $L \cdot F_{\mathbf{x}_i \to \mathbf{x}_j}$ is asymptotically χ^2 distributed [2,14], where L is the length of the time series. Therefore, we can use statistical tests (e.g., $p = 0.001$) to determine a GC threshold F_T [2] for constructing an effective adjacency matrix $\hat{\mathbf{A}} = (\hat{A}_{ij})$; i.e., if $F_{\mathbf{x}_i \to \mathbf{x}_j} > F_T$, we set $\hat{A}_{ji} = 1$, and otherwise, $\hat{A}_{ji} = 0$. For our two-neuron network, the adjacency matrix is successfully reconstructed in this way, as shown in Fig. 1(b). We further examine how robust this reconstruction is by scanning f and μ, which control the dynamical regimes, with the range over the realistic firing rates (5–150 Hz) of real neurons [15]. As shown in Fig. 1(c), the GC connectivity and the structural connectivity are highly coincident with each other. For a network of multiple neurons, we compute conditional GC ($F_{\mathbf{x}_i \to \mathbf{x}_j | \mathbf{x}_k}$) from x_i to x_j when the information of other nodes x_k ($k \neq i, j$) is given [2,14]. By using a significance test, $\hat{\mathbf{A}}$ can also be constructed. For a five-neuron network in Fig. 1(d), the constructed $\hat{\mathbf{A}}$ as shown in Fig. 1(e) is identical to $\mathbf{A}$. This method is also successfully tested to reconstruct $\mathbf{A}$ with 98% accuracy for a network of 100 excitatory neurons with random connectivity. Incidentally, we point out an interesting phenomenon for large excitatory-neuron networks: often, there is a gap in the GC ranked by magnitude for all possible directed connections between neurons, as shown in Fig. 1(f), and this gap clearly divides the GC values into two groups. Surprisingly, using this criterion [with the gray (red) horizontal line in Fig. 1(f) as the threshold], $\hat{\mathbf{A}}$ is also identical to $\mathbf{A}$.

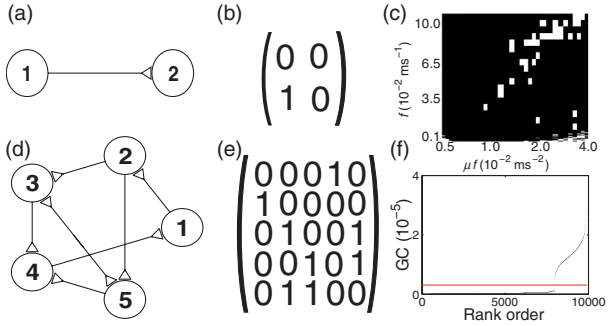

FIG. 1 (color online). (a) A network with two excitatory neurons and a directed connection from x_1 to x_2. (b) Effective adjacency matrix $\hat{\mathbf{A}}$ constructed by GC, which captures the structural connectivity in (a). (c) The coincidence between $\hat{\mathbf{A}}$ and $\mathbf{A}$ in (a) as a function of rate μ and magnitude f in the Poisson drive. The white color indicates that $\hat{\mathbf{A}} \neq \mathbf{A}$ and the black color for $\hat{\mathbf{A}} = \mathbf{A}$. (d) A network with five excitatory neurons. (e) $\hat{\mathbf{A}}$ constructed by GC, which captures the topology in (d). (f) Ranked GC in order of magnitude for a network of 100 excitatory neurons with random connectivity (the number of nonzero A_{ij} is ~2000). The gray (red) line indicates the threshold in the gap of the ranked GC. As for the excitatory neuron case, parameters are chosen as $x_{\rm ex} = 14/3$, $\sigma^{\rm ex} = 2$ ms, $\tau = 20$ ms, $x_{\rm th} = 1$, $x_r = 0$, and $\tau_{\rm ref} = 2$ ms [13]. Here, $\mu = 1$ ms^{-1}, $f = 0.007$ ms^{-1}, and $S^{\rm ex} = 0.01$ ms^{-1}.

Finally, we now turn to the question of why the linear GC framework is effective in uncovering the structural connectivity of nonlinear I&F networks. From the theoretical basis of GC analysis, one may suspect that an I&F system, albeit nonlinear, might be well described by a Gaussian linear regression process; i.e., the residuals in the above regression model might be Gaussian. Figure 2(a) shows the trajectories

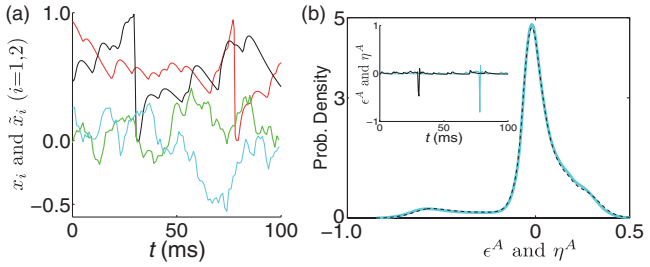

FIG. 2 (color online). (a) Trajectories of x_1 [thin dark line (red)] and x_2 [dark line (black)] generated by model (1) and of $\tilde{x}_1$ [thick gray line (green)] and $\tilde{x}_2$ [thick light gray line (cyan)] generated by regression models. (b) Probability density of ϵ^A [thick solid light gray line (cyan)] and η^A [thin dark dashed line (black)] in the AR model. Inset: Trajectories of ϵ^A [thick light gray line (cyan)] and η^A [thin dark line (black)]. Here, $\mu = 0.24\ \mathrm{ms}^{-1}$, $f = 0.02\ \mathrm{ms}^{-1}$, and $S^{\mathrm{ex}} = 0.01\ \mathrm{ms}^{-1}$.

of x_1 and x_2 from which we constructed regression processes to obtain the residuals ϵ^A and η^A. Figure 2(b) displays the probability density of ϵ^A and η^A, which are clearly not Gaussian. Note that, as shown in Fig. 2(a), the time series $\tilde{x}_1(t)$ and $\tilde{x}_2(t)$ (mean zero), which are reconstructed via the regression model of x_1 and x_2 with residuals replaced by Gaussian variables, are rather different from the original voltage series. Clearly, they have lost firing-reset signatures. However, it is important to point out that GC computed using $\tilde{x}_i$ can be shown to be identical to those GC obtained directly from x_i. In this sense, the I&F dynamics can be linearized statistically as captured by the regression process.

For pulse-coupled dynamical systems (e.g., I&F networks), the spike-triggered correlation is often used to infer connections in such systems [16]. The STC from x_1 to x_2 is defined as $x_2|_1(\tau) = \langle x_2(\tau_{x_1,k} + \tau)\rangle$, where $\tau_{x_1,k}$ is the kth spike time for x_1 and $\langle\cdot\rangle$ is the average over all spikes. Note that (i) the STC contains information about both the statistics of the spike drive from x_1 and the response properties of x_2, and (ii) such drive-response (causal) scenarios rely on the existence of a connection from x_1 to x_2; i.e., $A_{21} = 1$. Thus, it appears that STC could be used to relate the structural connectivity to the GC connectivity. Figure 3(a)

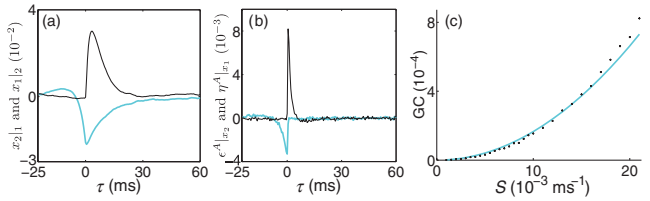

FIG. 3 (color online). (a) Spike-triggered correlation (background subtracted): $x_1|_2(\tau)$ [thick light gray line (cyan)] and $x_2|_1(\tau)$ [thin dark line (black)]. (b) Spike-triggered correlation: $\epsilon^A|_{x_2}(\tau)$ [thick light gray line (cyan)] and $\eta^A|_{x_1}(\tau)$ [thin dark line (black)]. (c) GC ("dot" symbols) as a function of coupling strength S^{ex}; the thick gray line (cyan) is a quadratic fit.

displays the STCs $x_1|_2(\tau)$ and $x_2|_1(\tau)$ (background subtracted), both of which exhibit significant deviations from zero when τ is small and naturally vanish when τ is sufficiently large. This might indicate bidirectional connections between the two neurons [16], however, which are inconsistent with the true structural connectivity ($A_{12} = 0$).

The nonzero feature of $x_1|_2(\tau)$ for $\tau > 0$ in Fig. 3(a), which gives rise to an incorrect inference of A_{12}, can be intuitively understood as follows. Because the signal $x_1(t)$ is not white, i.e., having finite correlation time, the future of x_1 is correlated with its own history. Further, $x_2(t)$ is also correlated with the history of x_1 (driven by its spikes). Therefore, $x_2(t)$ would likely be correlated with the future of x_1, hence the incorrect inference of the connection from x_2 to x_1.

Note that after regression, $\epsilon^A(t)$ and $\eta^A(t)$ are whitened signals [2], i.e., with only instantaneous correlation. Using STCs on ϵ^A and η^A, we have $\epsilon^A|_{x_2}(\tau) = 0$ for $\tau > 0$, as shown in Fig. 3(b), whereas $\eta^A|_{x_1}(\tau) \neq 0$ [similar features to $x_2|_1(\tau)$]. Therefore, the STC on whitened signals indicates the correct unidirectional connection between two neurons. This motivates us to study the relation between STC and GC on whitened signals. In the following, we show that the residual cross correlation r_τ, $r_\tau = \mathbb{E}[\epsilon^A(t)\eta^A(t+\tau)]$, links STC to GC.

First, we note that due to the firing-reset dynamics, the magnitude of ϵ^A at time $\tau_{x_1,k}$ is much larger in an absolute value than that at other times, as can be seen from the inset of Fig. 2(b), which resembles a Dirac delta function, i.e., $\epsilon^A(t) \approx -h\sum_k \delta(t - \tau_{x_1,k})$, where h is a normalizing factor. Under this approximation, we obtain the relation between r_τ and the STC on η^A,

$$\eta^A|_{x_1}(\tau) = \langle \eta^A(\tau_{x_1,k} + \tau)\rangle \approx -\frac{r_\tau}{h\nu}, \tag{2}$$

where ν is the spike rate of neuron 1.

Next, from AR models, we can construct the moving average of x_1 and x_2 in terms of ϵ^A and η^A [14] to obtain the JR models with respect to ϵ^A and η^A as follows:

$$\begin{aligned} \epsilon^A_n &= \sum_k \hat{a}^J_k \epsilon^A_{n-k} + \sum_k \hat{b}^J_k \eta^A_{n-k} + \epsilon^J_n, \\ \eta^A_n &= \sum_k \hat{c}^J_k \epsilon^A_{n-k} + \sum_k \hat{d}^J_k \eta^A_{n-k} + \eta^J_n, \end{aligned} \tag{3}$$

where (ϵ^A_n, η^A_n) and (ϵ^J_n, η^J_n) are the residuals in the original AR and JR models of x_i, respectively [17]. Note that the transformations between x_1, x_2 and ϵ^A, η^A are linear. By the invariance of GC under an invertible linear transformation [2], we have $F_{\epsilon^A \to \eta^A} = F_{\mathbf{x}_1 \to \mathbf{x}_2}$; i.e., GC connectivity is indeed embedded in the whitened signals.

Finally, from Eq. (3), we can construct and solve the Yule-Walker equations [14] and arrive at $F_{\mathbf{x}_1 \to \mathbf{x}_2} = -\ln(1 - r_i G_{ij} r_j)$ [18]. Here, $r_k = \mathbb{E}(\epsilon^A_n \eta^A_{n+k})$ and $(G^{-1})_{ij} = \mathrm{Var}(\epsilon^A)\mathrm{Var}(\eta^A)\delta_{ij} - R_{ik}R_{jk}$, with $R_{ij} = \mathbb{E}(\epsilon^A_n \eta^A_{n+i-j})$. For small residual cross correlation between

ϵ^A and η^A, which is consistent with the result in our numerical simulation of the I&F systems, $F_{\mathbf{x}_1\to\mathbf{x}_2}$ becomes

$$F_{\mathbf{x}_1\to\mathbf{x}_2} \approx \frac{r_k r_k}{\mathrm{Var}(\epsilon^A)\mathrm{Var}(\eta^A)}, \tag{4}$$

which links GC to STC quadratically through Eq. (2). Therefore, we can obtain that $F_{\mathbf{x}_1\to\mathbf{x}_2} \neq 0$ is equivalent to $\eta^A|_{x_1}(\tau) \neq 0$ for $\tau > 0$.

Note that $\eta^A|_{x_1}(\tau)$ corresponds to the spike-induced change which is asymptotically proportional (when τ is small) to the coupling strength S^{ex} by Eq. (1). Therefore, from Eqs. (2) and (4), we can make a final connection that GC is quadratically related to the coupling strength $F_{\mathbf{x}_1\to\mathbf{x}_2} \propto (S^{\mathrm{ex}})^2$, which is verified in Fig. 3(c). We point out that it is the δ-like noise structure of residuals, induced by the firing-reset dynamics, that links STC with the cross correlation [Eq. (2)]. This is a crucial feature in the I&F dynamics that underlies why the GC connectivity can be captured by the STC on whitened signals. The quadratic relationship between GC and S^{ex} [Fig. 3(c)] ultimately underlies the coincidence between the causal and the structural connectivities for the I&F networks.

Finally, we turn to the discussion of networks with both excitatory and inhibitory neurons. Figure 4 shows that in such cases, the GC connectivity is also highly coincident with the structural connectivity. For inhibitory connection, say, from the jth neuron to the ith neuron, although the voltage of the ith neuron will decrease after receiving the jth neuron's spike, both the δ-like noise structure and the firing-reset voltage dynamics are still preserved. Therefore, our theoretical analysis is also valid for networks with both excitatory and inhibitory connections.

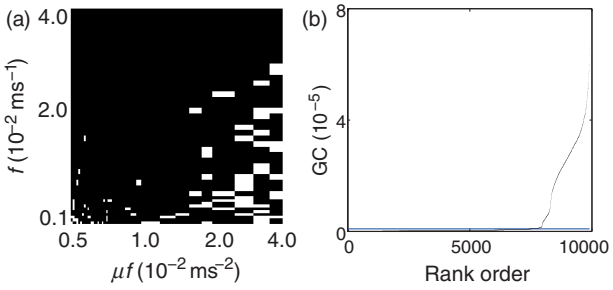

FIG. 4 (color online). (a) The coincidence between the structural adjacency matrix $\mathbf{A}$ and the effective adjacency matrix $\hat{\mathbf{A}}$ for a network with two inhibitory neurons. The network structural connectivity is the same as that in Fig. 1(a). The white color indicates that $\hat{\mathbf{A}} \neq \mathbf{A}$ and the black color that $\hat{\mathbf{A}} = \mathbf{A}$. (b) Ranked GC in order of magnitude for a network with 80 excitatory and 20 inhibitory neurons. Each matrix entry A_{ij} is randomly chosen as either zero or one (the number of nonzero A_{ij} is $\sim$2000). The gray (blue) line indicates the GC threshold F_T obtained from the p-value ($p = 0.001$) test. The accuracy of reconstruction is $\sim$96%. For the inhibition, parameters are chosen as $x_{\mathrm{in}} = -2/3$ and $\sigma^{\mathrm{in}} = 5$ ms [13]. Here, $\mu = 0.24\ \mathrm{ms}^{-1}$, $f = 0.02\ \mathrm{ms}^{-1}$, and $S^{\mathrm{in}} = 0.01\ \mathrm{ms}^{-1}$.

In summary, we have shown that the linear GC framework can indeed be applied to the pulse-coupled nonlinear network whose GC connectivity directly corresponds to its structural connectivity. We have also established a quantitative relationship among the GC, the STC, and the coupling strength. Our results are robust, provided that the time series are reasonably long ($\sim$ 20 min) [10] to reduce statistical errors. Our additional simulations show that a directed connection from one neuron to a subnetwork, or from one subnetwork to another subnetwork, can also be accurately detected by GC. Here, the recorded time series of a subnetwork is represented by the response (including spikes) averaged over its population, which can be viewed as a model for the local field potential in experiments [15]. We point out that if the averaged response is processed by a low-pass filter, our construction is still valid as long as the filter is causal. In addition, we have found that the structural connectivity can also be obtained via GC if we use spike trains (digital signals). Therefore, the GC tool can be directly applied to point-process data [3] for the pulse-coupled nonlinear networks. For networks with more realistic neuron models, e.g., the exponential I&F model, we find that our conclusions also remain valid. The above analysis of the mechanism for two nodes can naturally be extended to the case of multiple nodes, the digital signals, as well as the exponential I&F model. It is expected that this analysis can also be extended to a wide class of pulse-coupled networks with a broad type of firing-reset dynamics, e.g., Hodgkin-Huxley neuronal networks. Finally, we point out that other important issues remain to be elucidated in the future, e.g., correlated inputs and the synchronization. Our study here shows that (i) highly accurate reconstruction can be achieved (>70%) if the correlation coefficient in inputs is less than 10% [19], and (ii) for a nearly synchronized regime, the reconstruction can be achieved by refining sampling.

D. Z. is supported by Shanghai Pujiang Program (Grant No. 10PJ1406300) and National Science Foundation in China (Grants No. NSFC-11101275 and No. 91230202) and D. C. by Grant No. NSF-DMS-1009575. All authors are supported by the NYU Abu Dhabi Research Institute Grant No. G1301. Y. X., Y. Z., and Z. X. were partially supported by an Undergraduate Research Program in Zhiyuan College at Shanghai Jiao Tong University. We thank Gregor Kovacic for a critical reading of the manuscript.

*cai@cims.nyu.edu

[1] S. Strogatz, Nature (London) **410**, 268 (2001); S. Boccaletti, V. Latora, Y. Moreno, M. Chavez, and D Hwang, Phys. Rep. **424**, 175 (2006).

[2] J. Geweke, J. Am. Stat. Assoc. **77**, 304 (1982); **79**, 907 (1984).

[3] M. Ding, Y. Chen, and S. L. Bressler, in *Granger Causality: Basic Theory and Application to Neuroscience*, Handbook of Time Series Analysis, edited by S. Schelter, M. Winterhalder, and J. Timmer, (Wiley-VCH, Berlin, 2006), pp. 437–460; A. G. Nedungadi, G. Rangarajan, N. Jain, and M. Ding, J. Comput. Neurosci. **27**, 55 (2009); S. Kim, D. Putrino, S. Ghosh, and E. N. Brown, PLoS Comput. Biol. **7**, e1001110 (2011); S. L. Bressler and A. K. Seth, NeuroImage **58**, 323 (2011).

[4] L. Barnett, A. B. Barrett, and A. K. Seth, Phys. Rev. Lett. **103**, 238701 (2009); S. Bressler and A. K. Seth, NeuroImage **58**, 323 (2011).

[5] P.-J. Lahaye, J.-B. Poline, G. Flandin, S. Dodel, and L. Garnero, NeuroImage **20**, 962 (2003); A. Roebroeck, E. Formisano, and R. Goebel, *ibid.* **25**, 230 (2005); L. A. Johnston, E. Duff, I. Mareels, and G. F. Egan, *ibid.* **40**, 504 (2008).

[6] G. Nolte, A. Ziehe, V. Nikulin, A. Schlögl, N. Krämer, T. Brismar, and K.-R. Müller, Phys. Rev. Lett. **100**, 234101 (2008); S. Haufe, V. V. Nikulin, K. R. Muller, and G. Nolte, NeuroImage **64**, 120 (2013).

[7] A. K. Seth, Network **16**, 35 (2005); J. Upadhyay, A. Silver, T. A. Knaus, K. A. Lindgren, M. Ducros, D.-S. Kim, and H. Tager-Flusberg, J. Neurosci. **28**, 3341 (2008); M. Rubinov and O. Sporns, NeuroImage **52**, 1059 (2010).

[8] C. J. Honey, O. Sporns, L. Cammoun, X. Gigandet, J. P. Thiran, R. Meuli, and P. Hagmann, Proc. Natl. Acad. Sci. U.S.A. **106**, 2035 (2009); J. Damoiseaux and M. Greicius, Brain Struct. Funct. **213**, 525 (2009); T. Kispersky, G. Gutierrez, and E. Marder, Neural Syst. Circ. **1**, 9 (2011); O. Stetter, D. Battaglia, J. Soriano, and T. Geisel, PLoS Comput. Biol. **8**, e1002653 (2012); D. Battaglia, A. Witt, F. Wolf, and T. Geisel, PLoS Comput. Biol. **8**, e1002438 (2012).

[9] E. Salinas and T. J. Sejnowski, Nat. Neurosci. **2**, 539 (2001); P. Fries, Trends Cogn. Sci. **9**, 474 (2005); X. J. Wang, Physiol. Rev. **90**, 1195 (2010).

[10] M. A. Koch, D. G. Norris, and M. Hund-Georgiadis, NeuroImage **16**, 241 (2002); J. R. Sato, E. A. Junior, D. Y. Takahashi, M. de Maria Felix, M. J. Brammer, and P. A. Morettin, NeuroImage **31**, 187 (2006); S. Hu and H. Liang, Neurocomputing **76**, 44 (2012).

[11] D. Marinazzo, M. Pellicoro, and S. Stramaglia, Phys. Rev. Lett. **100**, 144103 (2008); Phys. Rev. E **77**, 056215 (2008).

[12] R. Mirollo and S. Strogatz, SIAM J. Appl. Math. **50**, 1645 (1990); D. C. Somers, S. B. Nelson, and M. Sur, J. Neurosci. **15**, 5448 (1995); T. W. Troyer, A. E. Krukowski, N. J. Priebe, and K. D. Miller, J. Neurosci. **18**, 5908 (1998); W. Mather, M. R. Bennett, J. Hasty, and L. S. Tsimring, Phys. Rev. Lett. **102**, 068105 (2009); Z. Wang, Y. Ma, F. Cheng, and L. Yang, Image Vis. Comput. **28**, 5 (2010).

[13] D. McLaughlin, R. Shapley, M. Shelley, and D. J. Wielaard, Proc. Natl. Acad. Sci. U.S.A. **97**, 8087 (2000); D. Cai, A. V. Rangan, and D. W. McLaughlin, *ibid.* **102**, 5868 (2005); A. V. Rangan, D. Cai, and D. W. McLaughlin, *ibid.* **102**, 18 793 (2005).

[14] S. Pandit and S. Wu, *Time Series and System Analysis with Applications* (Wiley, New York, 1983); A. McQuarrie and C.-L. Tai, *Regression and Time Series Model Selection* (World Scientific, New Jersey, 1998).

[15] P. Dayan and L. Abbott, *Theoretical Neuroscience* (MIT Press, Cambridge, MA, 2001); W. Gerstner and W. Kistler, *Spiking Neuron Models* (Cambridge University Press, Cambridge, England, 2002); X. Jia and A. Kohn, PLoS Biol. **9**, e1001045 (2011).

[16] E. de Boer and P. Kuyper, IEEE Trans. Biomed. Eng. **BME-15**, 169 (1968); M. Matsumura, D.-f. Chen, T. Sawaguchi, K. Kubota, and E. E. Fetz, J. Neurosci. **16**, 7757 (1996); U. Bhalla, PLoS Comput. Biol. **4**, e1000098 (2008).

[17] Equation (3) can also be obtained by least-squares methods.

[18] Tensor notations and the Einstein summation are used.

[19] R. Gütig, R. Aharonov, S. Rotter, and H. Sompolinsky, J. Neurosci. **23**, 3697 (2003).